Electronic band structure of ordered Cu_3Au: An angle-resolved photoemission study along the [001] direction

R. Courths and S. Löbus
Laboratorium für Festkörperphysik, Fachbereich Physik, Universität Duisburg, D-47048 Duisburg, Germany

S. Halilov, T. Scheunemann, H. Gollisch, and R. Feder
Theoretische Festkörperphysik, Fachbereich Physik, Universität Duisburg, D-47048 Duisburg, Germany

(Received 24 February 1999)

High-resolution angle-resolved ultraviolet photoemission spectra (ARUPS) have been recorded for $Cu_3Au(001)$ with the use of polarized synchrotron and rare-gas resonance radiation in the photon energy range 9–26 eV. A fully relativistic layer–Korringa-Kohn-Rostoker formalism was employed to calculate the initial- and final-state bulk band structure as well as one-step model photoemission spectra. Hole and photoelectron lifetime effects are taken into account. The calculated empty bulk bands along the [001] direction (Δ line in $\vec{k}$ space), which carry most of the electron flux into the normal direction along [001], were—after a real self-energy correction of $+2.5$ eV—used to perform an experimental band mapping. The thus determined occupied Cu-like *d* bands and the *sp* band are in good agreement with the calculated ''Kohn-Sham bands,'' if the latter are shifted downward in energy by 0.3 eV. For the Au-like *d* bands, some deviations persist. Measured ARUPS spectra agree well with their calculated counterparts, which corroborates our identification of direct bulk transition features and our band mapping. In addition, numerous features are found to arise from surface states or resonances. Normal-incidence inverse photoemission data taken for $h\nu = 9.7$ eV further support our findings. [S0163-1829(99)07835-2]

I. INTRODUCTION

The noble-metal binary alloy Cu_3Au has attracted much attention because of the classical order-disorder phase transition found at 663 K. In this context, the electronic structure is a key quantity of great interest. The bulk band structure of Cu_3Au has therefore been studied in a number of theoretical papers by first-principles approaches (Davenport *et al.*,[1] Weinberger *et al.*,[2] Ginatempo *et al.*,[3] Sohal *et al.*,[4] Kudrnovsky *et al.*,[5] Lu *et al.*,[6] Halilov *et al.*,[7] and references therein). The basic characteristics of the electronic structure of the occupied valence bands have been discussed in detail in the paper of Lu *et al.*[6] For convenience, we summarize some of the most important features of ordered Cu_3Au in terms of the densities of states (DOS) presented in Fig. 1 (calculational details are given below). The Au $5d$ states narrow and shift away from the Fermi level as compared to pure Au, whereas the energies of the Cu $3d$ states are much weaker influenced. Due to the hybridization of Cu and Au states, none of the band states is of pure Cu or Au atomic origin. The large spin-orbit coupling of Au also enhances the mixing of states. Thus, the Cu and Au atoms share a common *sp* band and common *d* bands where the hybridization is considerable. Although the atomic character of the band states is not pure, it is nevertheless meaningful to distinguish between Au-like bands between 7- and about 5-eV energy below E_F (region ''Au'' in Fig. 1) and Cu-like bands between about 4 and 1.5 eV (''Cu''), respectively. The mixing is especially pronounced in the region between the Cu-like and Au-like bands (''*M*''). The band structure of the Cu-like bands is rather complex because of backfolding effects due to the reduction of the fcc Brillouin zone (BZ) of pure copper to the smaller simple cubic BZ of Cu_3Au.

Among the experimental methods for probing the bulk electronic structure (a collection of references up to 1992 can be found in the contribution of Lu *et al.*[6]), angle-resolved photoelectron spectroscopy (ARPS), especially with photon energies in the VUV regime [angle-resolved ultraviolet photoemission spectroscopy (ARUPS)], plays a dominant role. In two previous papers (Sohal *et al.*[4] and Wang *et al.*[8]) ARUPS measurements were used to perform a band mapping of $Cu_3Au(001)$ along the [001] direction. The data points thus obtained exhibit, however, a fairly large scatter, which prevents a detailed comparison with calculated *d* bands. Furthermore—in contrast to the case of pure copper (see, for example, Courths and Hüfner[9])—emission from the *sp* band near the Fermi energy was found to be very weak and only a few data points were obtained for this *sp* band. On the other hand, our ARUPS study of $Cu_3Au(111)$ (Ref. 10) succeeded in a very detailed mapping of both the Cu-like and the Au-like valence bands along the [111] direction in good agreement with their calculated counterparts.

The comparatively unsatisfactory situation for the bulk bands of Cu_3Au along the [001] direction has motivated the present thorough investigation by means of ARUPS measurements in conjunction with theory. Some preliminary results have already been given in a recent publication[11] which has mainly been devoted to the identification and characterization of surface states on the (001) surface of Cu_3Au.[11] In that work we have given experimental evidence for the existence of a wealth of surface states and resonances which partly dominate the ARUP spectra (depending on the photon energy used). Their identification was therefore a necessary step prior to mapping the bulk bands.

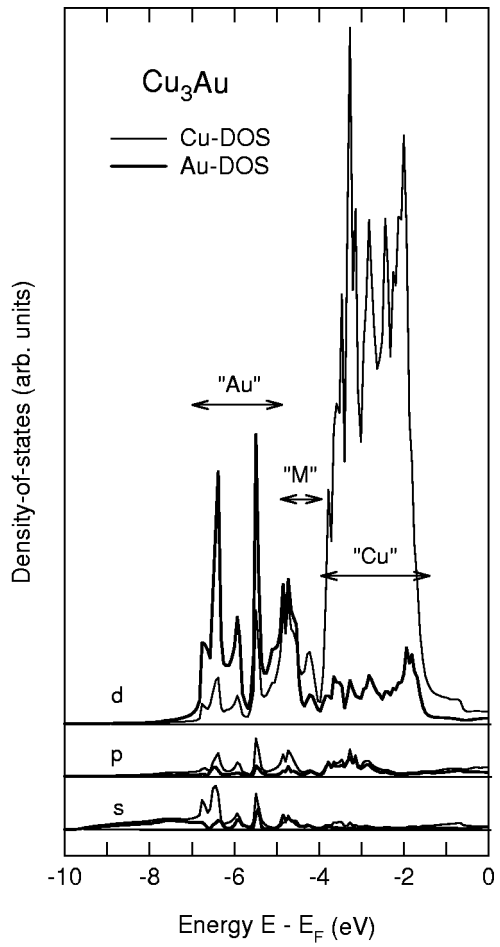

FIG. 1. Atom- and angular-momentum-resolved total densities of states of Cu_3Au. Cu: thin lines. Au: thick lines.

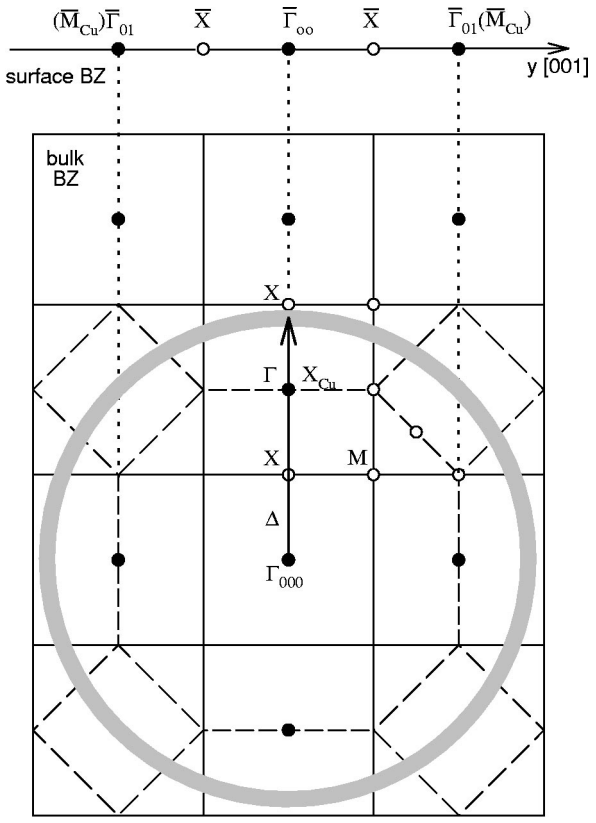

FIG. 2. Cut of the bulk Brillouin zones (BBZ) of Cu_3Au and fcc Cu (dashed lines and index Cu at the symmetry point labels) along the (100) plane through the center assuming the same lattice constants. The centers of the BBZ's of Cu_3Au are indicated by the filled circles. The dotted lines indicate the projections of bulk symmetry points onto the $\bar{\Gamma}$-$\bar{\Delta}$-$\bar{X}$ line of the (001) surface BZ. The shaded ring roughly marks the region in $\vec{k}$ space which is most relevant for photoemission with $h\nu \approx 20$ eV from initial states of energies $E_i \approx -2$ eV (for details see text). In particular, the arrow represents the dominant wave vector $\vec{K} = \vec{k} + \vec{G}$ of a direct transition near the X point of the BBZ.

The use of angle-resolved photoemission for the determination of bulk and surface electronic bands of single crystals, its successes and difficulties have been reviewed in several articles.[9,12,13] The occupied bands and their dispersions are determined by observing direct interband transitions, which are swept over the Brillouin zone (BZ) by using tunable synchrotron radiation. One of the major problems is the location of the direct transitions in $\vec{k}$ space, because the component of the wave vector $\vec{K} = \vec{k} + \vec{G}$ of the photoelectron ($\vec{k}$ is the reduced wave vector and $\vec{G}$ is a reciprocal-lattice vector) perpendicular to the surface $\vec{K}_\perp$ is not conserved in the photoemission process. Figure 2 displays the Brillouin-zone structure of the emission plane in $\vec{k}$ space used in this work. Free-electron- (FE-) like bands are often used as final state,[9] which requires a good guess for the effective mass and the zero potential. However, these quantities are not well defined. In addition, the FE approximation often yields distorted band dispersions due to the bad approximation to the dispersion of the ''true'' final state, especially near the band gaps of the unoccupied band structure calculated with a real potential. By way of illustration, the shaded ring in Fig. 2 gives the $\vec{k}$-space location of the FE final states of energy $E_{f,FE} = E_i + h\nu$, which are reached at photon energy $h\nu \approx 20$ eV from initial states with energies $E_i \approx 2.0$ eV on a ring with a radius K slightly less than the distance Γ-X. The correct final-state wave vector $\vec{K}$ and hence the radius of the ring is not known *a priori* but has been taken from our results given in Sec. IV. For smaller photon energies, $\vec{K}$ decreases. It is thus plausible that photon energies between about 10 and 20 eV map the bands along $\Gamma - \Delta - X$ in the second Brillouin zone of $Cu_3Au(001)$. While a free-electron final state involves a fairly crude approximation, the use of calculated unoccupied (final-state) bands, with proper adjustment in energy, has been shown to yield much better results.[9,14,15] However, care has to be taken near the critical points Γ and X where gaps of the unoccupied bands are bridged by ''gap states'' (so-called ''gap emission'';[14] to be discussed in Chap. IV). Part of our present work focuses on this problem. More direct contact between experiment and theory can be made by comparing measured PE spectra with their counterparts calculated within a one-step model, which includes both excitation and electron damping. In this paper we also present such comparison.

II. EXPERIMENTAL

The experiments were performed at the synchrotron light source BESSY in Berlin on beamline TGM2, using photons

with energies 9 eV $\leqslant h\nu \leqslant 41$ eV, and in our home laboratory, using Ne and He resonance radiation. As photoelectron spectrometers an ADES 400 system (BESSY) and an ESCALAB system from Vacuum Generators were used. For the synchrotron radiation experiments the total-energy resolution (photons plus electrons, full width) was about 80 meV for 9 eV $\leqslant h\nu \leqslant 24$ eV and increased to about 150 meV at the highest photon energy, whereas for the laboratory experiments the resolution was about 60 meV. The electron angular resolution was about 3° (full angle of acceptance).

Electrons were collected along the surface normal (z or [001] direction) of $Cu_3Au(001)$. The measuring plane was the (100) yz mirror plane. The coordinates used in this paper are given in Fig. 2. The photons were incident in that mirror plane with an angle Θ_{ph} with respect to the surface normal. The linearly polarized synchrotron light ($\cong 90\%$ degree of polarization) was oriented in the plane of incidence (p or yz polarization) and photoemission spectra were taken with $\Theta_{ph}=62°$ [$z(y)$ light] and $\Theta_{ph}=20°$ [$y(z)$ light], respectively, in order to vary the electric-field components perpendicular (z) and parallel (y) to the surface. The light from the resonance lamps was incident at $\Theta_{ph}=40°$ in the yz plane and was either unpolarized or $yz(p)$ or $x(s)$ polarized with about 90% degree of polarization.

Angle-resolved inverse photoemission (ARIPE) spectra were collected in the isochromat mode at $h\nu=9.7$ eV with normally incident electrons. The photons were collected by an elliptical mirror around the surface normal and the flux was measured using a Dose-type counter. The total-energy resolution was about 800 meV.

The single crystal of ordered $Cu_3Au(001)$ was cleaned *in situ* by repeated cycles of Ar^+-ion bombardment ($\cong$500-eV beam energy) and subsequent annealing up to 640 K (below the phase-transition temperature of 663 K) for several hours. This procedure was done until sharp superstructure low-energy electron diffraction (LEED) spots [a $c(2\times2)$ structure as compared with the Cu(001) LEED pattern] indicated a well-ordered surface at room temperature. The intensity and the energetic position of the photoelectron emission from the Tamm-type surface state at 1.53 eV below the Fermi energy (Refs. 11 and 16) was also used to check the quality and the orientation of the surface with respect to the analyzer. The chemical cleanliness of the surface was checked by means of x-ray excited core-level emissions (XPS) (home experiments). In addition, angle-resolved photoelectron spectra from a Cu(001) sample were measured for comparison.

III. THEORETICAL

The electronic structure of the ground state of bulk Cu_3Au (with the experimental lattice constant of 3.748 Å) was self-consistently calculated by the linear muffin-tin orbital (LMTO) method within the framework of Nobel prize-winning density-functional formalism with a local-density exchange-correlation approximation.[17] The calculations were scalar relativistic throughout the self-consistency cycle, but spin-orbit coupling was included in the last step. In each step, the atomic sphere radii were chosen to ensure charge neutrality. The final radii for Au and Cu are 1.63 and 1.40 Å, respectively. The inner potential is 15.05 eV (below the vacuum level).

The resulting occupied one-electron energy bands, which have already been shown in earlier work,[7,11] essentially agree with those obtained and discussed in detail by other groups.[1–4] There are, however, some differences, which we attribute mainly to different values of the atomic sphere radii. In particular, our Cu-like bands are about 0.15-eV lower in energy.

For the purpose of analyzing and interpreting our experimental photoemission data, we further calculated an unoccupied one-electron bulk band structure as well as one-step-model photoemission spectra. To these ends, we employed a fully relativistic layer–Korringa-Kahn-Rostoker- (KKR-) type Green-function formalism for semi-infinite crystalline ferromagnetic systems, which has been presented in Ref. 18. This formalism can handle several atoms per unit cell. Further, it incorporates the hole lifetime from the start.

The effective one-electron potential for the layer-KKR calculations was constructed by firstly casting the (real) LMTO potential into the muffin-tin form. The radii of the touching Au and Cu spheres were chosen such as to minimize discontinuities, which gave values 1.39 and 1.23 Å, respectively. The occupied bulk energy bands obtained from this muffin-tin potential by our layer-KKR method are practically the same as those from the original LMTO calculation.

It is important to note that the above muffin-tin potential is the Kohn-Sham one-electron potential of the ground state. To describe the quasiparticle states, which are relevant for photoemission, its real uniform part V_{or} has in general to be modified by energy-dependent self-energy corrections for the lower and the upper state. In the absence of first-principles knowledge, we presently take these corrections, which correspond to shifting the lower and the upper bands, as parameters to be determined by comparison with our experimental photoemission data.

Furthermore, quasiparticle lifetimes are taken into account by means of uniform imaginary potential parts for both the lower and the upper states. For occupied states of energy E_1, we choose $V_{i1}=-(E_1-E_F)\times 0.025$ eV, i.e., a form linearly increasing in magnitude away from the Fermi energy E_F. For the unoccupied states of energy E_2 relative to the vacuum level E_{vac}, we use the form $V_{i2}=-2.5/\{1+\exp[-(E_2-22.61)/6.78]\}+0.49$ eV, which is suggested by LEED experience (cf. Ref. 19, Chap. 4). For the kinetic energies E_2 from E_{vac} to about 15 eV, which are reached in our present photoemission study, the values of this V_{i2} range from -0.5 eV to -1.0 eV. We note that the value -1.0 eV for $E=15$ eV is close to the one determined by a photoemission experiment.[20]

IV. RESULTS AND DISCUSSION

A. Density of states

We start the presentation of our results by demonstrating by experiment the validity of the division of the valence states in Cu-like and Au-like states, respectively. In Fig. 3 we show a series of PE spectra, which we have measured for photon energies in the range 20–150 eV, covering several Brillouin zones along [001] (see Fig. 2), and compare them

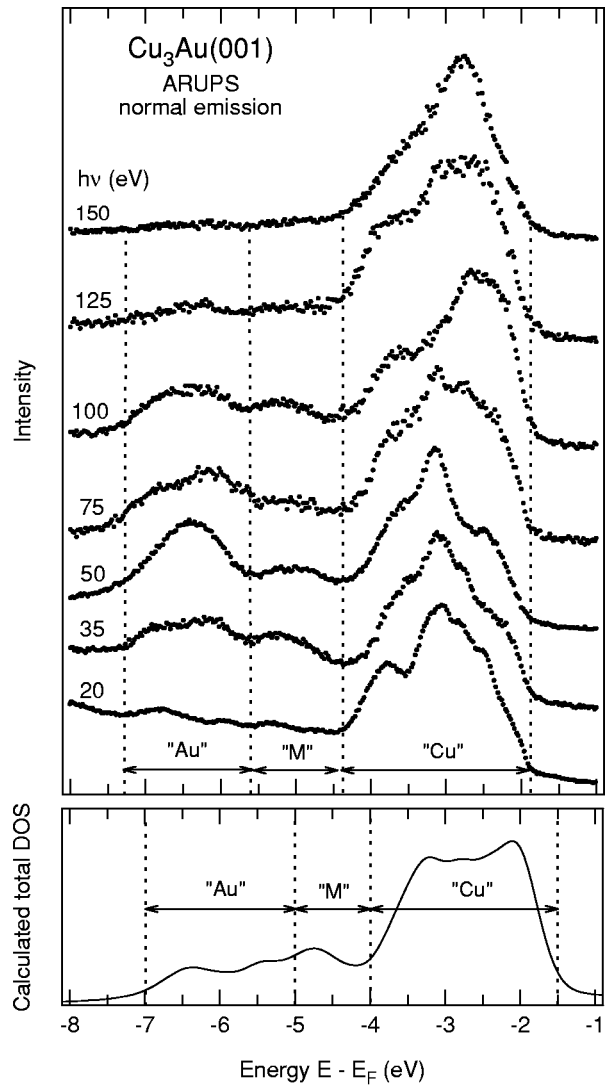

FIG. 3. Above: Series of normal-emission photoemission spectra for $Cu_3Au(001)$ with photon energies between 20 and 150 eV. Below: Smoothed total density of states. For details see text.

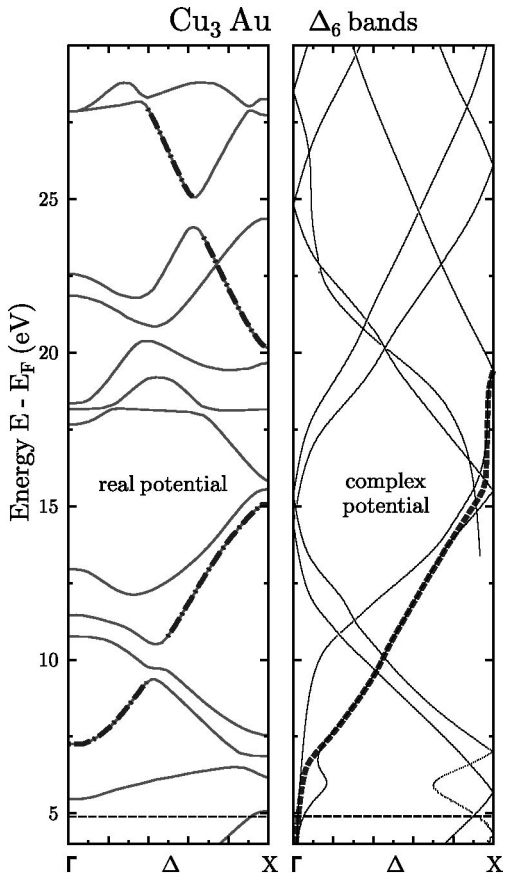

FIG. 4. Unoccupied ground-state band structure for Cu_3Au along the [001] direction (Δ line in $\vec{k}$ space) with double group symmetry Δ_6 calculated for the real ground-state potential V_r (left panel) and for the complex potential $V_r + V_{im}$ (right panel). In the left panel, the bold dash-dotting emphasizes the Δ_6 band parts which carry most of the electron flux along the [001] surface normal of $Cu_3Au(001)$. In the right panel, the bold dashes represent an effective flux-carrying band, which in its central part and in its upper and lower parts follows two different calculated bands; further it contains two smooth transition parts between these two bands.

with the calculated total bulk DOS. The spectra have been normalized to equal integral intensity between -4.5 and -2 eV energy below E_F. Compared to that energy range the emission below -4.5 eV has low strength at low and high photon energies, but has considerable strength in between and particularly around $h\nu = 50$ eV. This intensity variation reflects the dependence of the Au $5d$ cross section for photoionization,[21] which is maximum at about 40 eV and slows down with increasing photon energy to a very weak Cooper minimum at around $h\nu = 210$ eV. Experimentally, the states with dominant Au $5d$ character are thus found between -7.3 and -5.7 eV (region ''Au''). Between -5.7 and -4.5 eV the mixing of Au and Cu states is considerable (region ''*M*''). The Cu-like states are found between -4.5 and -2.0 eV (region ''Cu''). Concerning the energy width of these three regions, the agreement with the calculated total DOS is very good. In order to take into consideration lifetime effects and the experimental resolution, the calculated DOS was first convoluted by an energy-dependent Lorentzian with half width V_{i1} (see the theory section) and subsequently by a Gaussian [of full width at half maximum (FWHM) = 0.33 eV]. As is evident from Fig. 3, overall good agreement with the experimental peak energies is obtained if the theoretical DOS is shifted downward in energy by about 0.3 eV.

Similar results have already been obtained by Eberhardt *et al.*,[22] Wertheim and co-workers,[23–25] Weinberger *et al.*,[2] Krummacher *et al.*,[26] and Sohal *et al.*[4] (all cited authors used photoemission experiments either in the angle-resolved or angle-integrated mode, the latter including XPS). In agreement with our finding, Wertheim *et al.*,[24] Weinberger *et al.*,[2] Krummacher *et al.*,[26] Sohal *et al.*,[4] and Lau *et al.*[10] have already pointed out that, in order to obtain better agreement between experimental and calculated valence-band energies, the latter have to be shifted downwards by a ΔE of some tenths of an eV relative to the Fermi energy E_F, since the calculated Fermi energy falls short by ΔE. The exact value of ΔE depends sensitively on the theoretical method used by the different authors, since for noble metals E_F lies in the sp band, which has a very small DOS. It should be mentioned that the spectra shown in Fig. 3 do not simply reflect the bulk

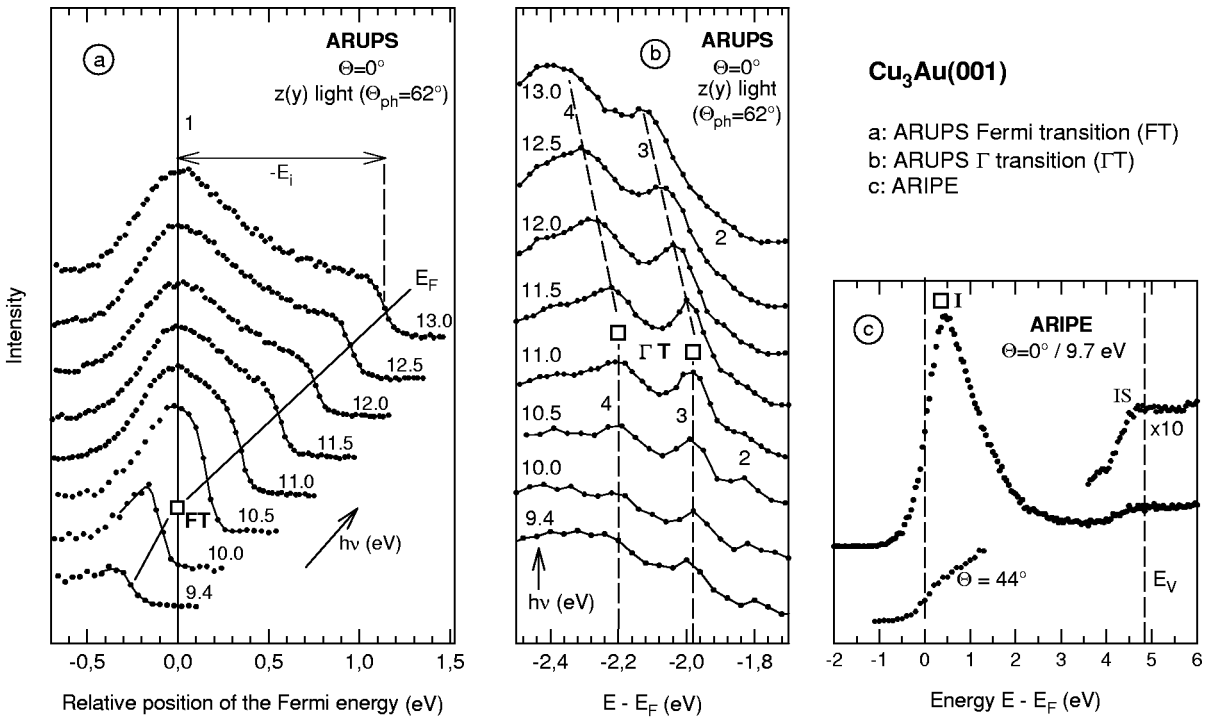

FIG. 5. Left panel: Series of normal-emission sp-band ARUP spectra taken from $Cu_3Au(001)$ with photon energies between 9 and 13 eV taken with synchrotron light with $z(y)$ polarization ($\Theta_{ph}=62°$). The sp-band features (1) have been aligned for the position of the low-energy side of the emission profile, which agrees with the alignment of the sp-band maximum visible above 10.5 eV [line (1)]. The line with the label E_F indicates the Fermi energy. The open square labeled FT (for Fermi transition) marks the sp-band excitation at the Fermi energy (Fermi level crossing), corresponding to 10.2-eV photon energy. Center panel: ARUP spectra for photon energies $h\nu$ as indicated. Prominent features are numbered by 2, 3, and 4. The two open squares labeled ΓT mark transitions near the Γ point. Right panel: Inverse photoemission spectrum for photon energy 9.7 eV and electron incidence along the surface normal and at polar angle $\theta=44°$, respectively. IS denotes an image state below the vacuum level E_V.

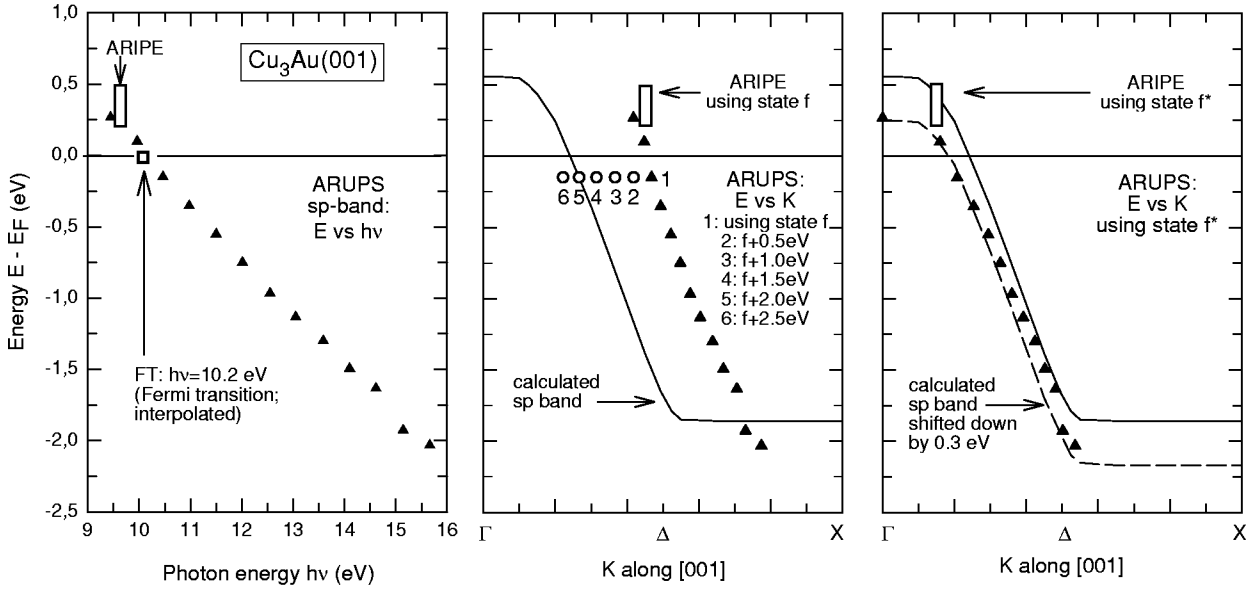

FIG. 6. Location of the sp-band photoemission feature (filled triangles), the Fermi transition (open square), and the ARIPE transition (open rectangular) in $\vec{k}$ space along [001]. Left: Energy dispersion of the sp-band feature 1 in Fig. 5 with photon energy. Center: Energy dispersion with wave vector $K_\perp$ in the second BZ (cf. Fig. 1), as obtained by using the final-state band in Fig. 4(b). The solid line represents the calculated sp band. Right: Same as in the center panel but obtained by using the upward-shifted final-state band f^*, which is shown in Fig. 7. The dashed line represents the calculated sp-band shifted down in energy by 0.3 eV.

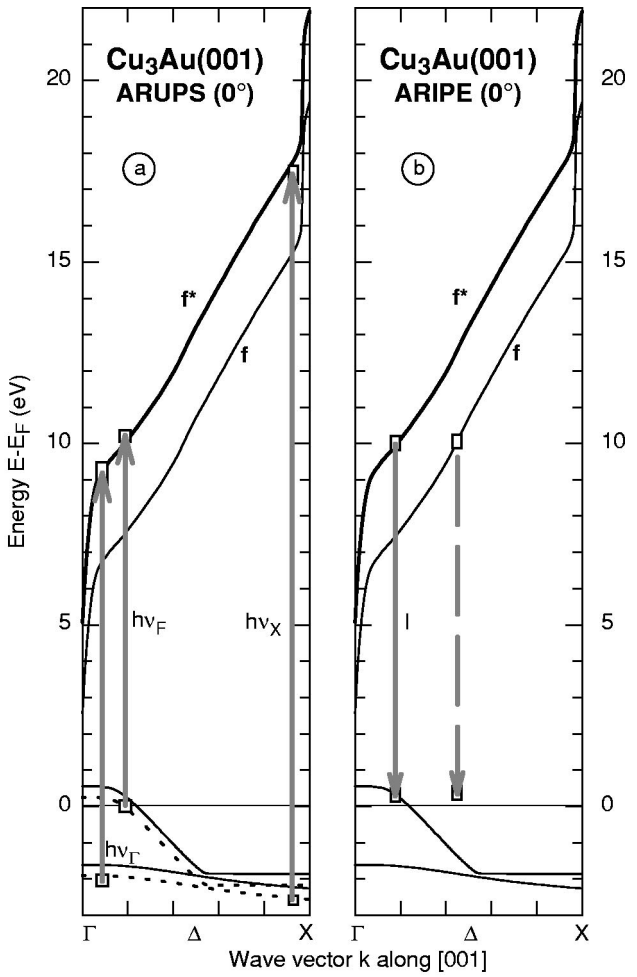

FIG. 7. Band structure of Cu_3Au along the [001] direction and possible direct interband transitions. The two uppermost occupied valence bands (including the unoccupied part of the *sp* band) are shown as calculated (thin solid lines) and shifted down by 0.3 eV (thin dashed lines). The upper-state band *f* (thin solid line) is the effective one from Fig. 4(b), and *f** (thick solid line) is the ''experimental'' upper-state band (used for band mapping in this work), which is obtained by shifting band *f* upward by 2.5 eV. In the left panel, arrows indicate some special ultraviolet photoemission spectroscopy transitions: the Fermi transition ($h\nu_F$), the Γ transition from the upper *d* band ($h\nu_\Gamma$), and the *X* transition from the lower *d* band ($h\nu_X$). In the right panel the arrow indicates the experimental IPE transition of Fig. 5 assuming two different upper states, namely, the calculated band *f* and the ''experimental'' band *f**, respectively.

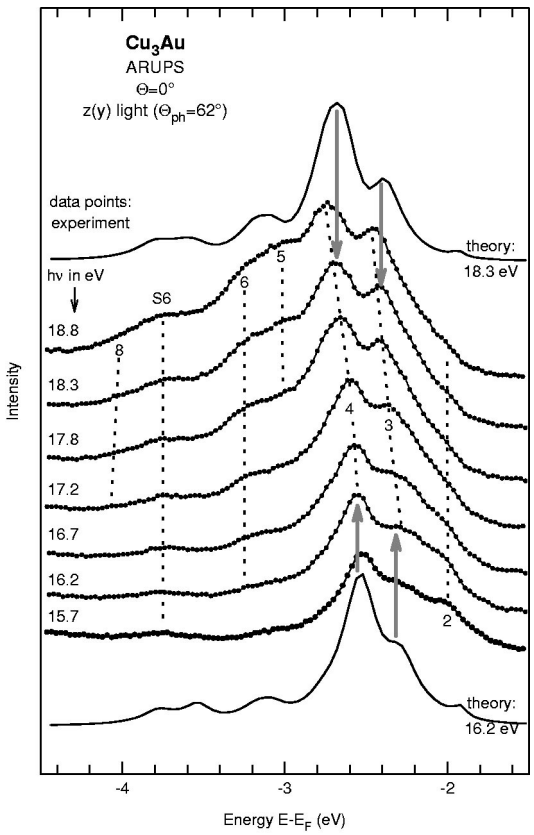

FIG. 8. Series of normal-emission ARUP spectra (data points) taken from $Cu_3Au(001)$ with photon energies between 15.7 and 18.8 eV and $z(y)$ polarized synchrotron light ($\Theta_{ph}=62°$) representing the emissions from the Cu-like *d* bands. The spectra drawn with solid lines were calculated within the one-step layer-KKR formalism, employing real self-energy corrections of 2.5 eV (upward shift) and -0.3 eV (downward shift) for the unoccupied and the occupied bands, respectively.

DOS, but contain more or less intense contributions from the surface DOS.[11,24,25,27] Surface emission is weak at the top of the Cu-like *d* bands, but can be rather strong within the Au, *M*, and Cu regions, depending on the photon energy. An example is the intense feature appearing at -6.3 eV around $h\nu=50$ eV in Fig. 3 (surface state S_9 in Ref. 11). From the experimental side there is thus no doubt that the top of the Cu-like bulk *d* bands is located near 2.0 eV, that the *d*-band width of the Cu-like states is about 2.5 eV and that the overall *d*-band width (Cu and Au bands) is about 5.0–5.5 eV. Worth mentioning is also the work of Stuck *et al.*,[28] who have displayed the atom-resolved DOS using the technique of XPD.

B. Final- (upper) state band structure

The calculated occupied bulk bands along the [001] direction have already been given in a recent paper[11] (see Ref. 10) for bands along [111]) and will be presented below together with the experimental band structure. In order to perform band mapping from the experimental photoemission data and to interpret the latter in a one-electron picture in terms of direct bulk interband transitions, the band structure of the final-state electrons is required.

In the left panel of Fig. 4 we show an upper band structure, which we calculated using simply the real one-electron potential obtained in the self-consistent ground-state calculation. Due to the relativistic selection rules,[29] only final states with $\Delta_{6(1)}$ symmetry (nonrelativistic notation is given in parentheses) are allowed to emit along the surface normal of an (001) terminated crystal. The thick dash-dotting emphasizes those $\Delta_{6(1)}$ bands, whose wave functions have a dominant contribution of wave vector $\vec{K}=\vec{k}(001)+\vec{G}(001)$ along the [001] surface normal and therefore carry most of the electron flux into the direction under investigation. The other Δ_6 bands result from backfolding and have low emission strength along [001]. Hence they can be neglected in first approximation for the evaluation of the experimental data.

As is well known, however, the upper states are more adequately described by quasiparticles, the complex self-energy of which accounts for many-body effects (cf. e.g., Ref. 30 and references therein). We recall that the real self-energy part can approximately be treated as an energy-dependent raising ΔV_r of the uniform inner potential. The imaginary self-energy part, which accounts for the lifetime of the photoelectron, can be taken into account by a uniform imaginary part V_i of the inner potential. The effect of ΔV_r on the band structure is simply an (energy-dependent) upward shift of the bands. We treat ΔV_r as a parameter to be determined with the aid of our experimental data. For the determination of the band structure of copper, unoccupied bands calculated with a ground-state potential have been used successfully as final states for bulk direct interband transitions in the low photon-energy regime[9] (see also Fig. 2 of Ref. 10), which means that ΔV_r is very small in copper. For the case of gold, however, it was necessary to apply a rigid energy shift of $+0.7$ eV to the unoccupied bands resulting from a ground-state potential to obtain the experimental occupied band structure.[15] It is therefore necessary to perform a careful adjustment of the theoretical final bands prior to its use as final states in angle-resolved photoemission. In our investigation of ARUPS from $Cu_3Au(111)$ (Ref. 10) we have found that a rigid shift of $+2.5$ eV has to be applied to the ''Kohn-Sham'' bands to yield a reliable experimental valence-band structure.

Photoelectron lifetime effects, which are always present in reality, have frequently been neglected, in many cases without too much harm. On the other hand, cases are known (cf. e.g., Ref. 31), where they play a crucial role. To assess their importance in the present context, we show in the right panel of Fig. 4 the real part of the complex band structure, which was calculated for the real ground-state potential augmented by an imaginary part V_{i2} as specified in Sec. III. The main effect of V_{i2} is a smearing out of gaps along the Δ line [e.g., the gap between the real potential bands at about 10 eV in Fig. 4(a)] and at the center (Γ point) and the border (X point) of the Brillouin zone. Near the critical points, the gaps are bridged by band segments, which have a very steep dispersion. Excitation into these bands segments explains the ''gap emission'' observed in many ARUPS experiments (see Ref. 14 and references therein). This disappearance of the gaps at the critical points (where the dispersion is not at all free-electron-like) and the rather free-electron-like dispersion along the Δ line in between the ''gap regions'' should be taken into account. Therefore the continuous band shown with bold dashes in the complex-potential band structure (which we denote as band f in the following) will be used as a template, besides an energy shift to be determined below, for the dominating final band. We will show below that the use of this band shifted by 2.5 eV to higher energy (which then is denoted as band f^*) explains our (001) photoemission spectra very well.

C. Emission from the *sp* band near the Fermi level, photoemission near critical points, inverse photoemission, and energy corrections for the calculated band structure

A key band-structure feature that can be determined without assumptions about the final band of a direct transition is

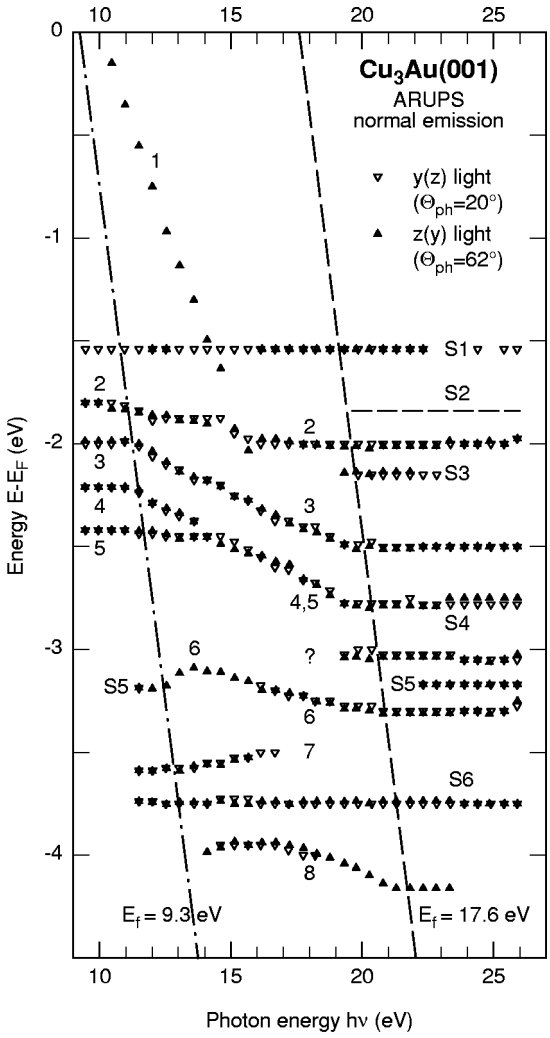

FIG. 9. Dispersion with photon energy of the Cu-like features in the experimental spectra.

the photon energy $h\nu_F$ for the transition between the lower and the upper branch of the sp band at the Fermi wave vector k_F (called Fermi transition or Fermi-level crossing in the following) along the [001] direction. This has been demonstrated by Eastman *et al.*[20,32] using normal photoemission from Cu(001) and by Himpsel and Ortega[33] using inverse photoemission from Cu(001), Ag(001), Au(001), and $Cu_3Au(001)$. This Fermi-level crossing is shown in Fig. 5(a), where a series of ARUP spectra from the occupied sp band near the Fermi energy (feature 1) are plotted. The dispersion of the sp-band feature with photon energy is given in the left panel of Fig. 6. As interpolated from these data, the Fermi transition occurs at $h\nu_F = 10.2$ eV, being in perfect agreement with the IPE result of Himpsel and Ortega.[33] For higher photon energies the center of the excitation, which is given by the vertical line in Fig. 5, is well below E_F and the feature has the common peak shape. In contrast, for photon energies lower than 10.2 eV the peak shape is deformed by the Fermi distribution and the center is above E_F.

The Fermi transition in the band structure is given in Fig. 7(a). The final state f^* is by about 2.5-eV higher in energy than the relevant band f in the calculated complex band structure, demonstrating that an unshifted band f cannot be used for a mapping of the occupied bands. In the center

panel of Fig. 6 we demonstrate the error in $\vec{k}$ space which results if one does not properly adjust the final band (triangles 1 and open circles 2–5). Using the uncorrected final band *f*, the $(E,\vec{k})$ points 1 are obtained as shown by filled triangles. Although the theoretical dispersion $dE/d\vec{k}$ of the calculated occupied *sp* band is well reproduced, which only demonstrates the correct dispersion of the final band *f*, the experimental points are displaced erranously, as compared to the calculated sp band, along $\vec{k}$ towards the *X* point by about 20% of $\overline{\Gamma X}$. Shifting band *f* successively by 0.5 eV the $E(k)$ points given by the open circles labeled 2–6 are obtained. Nearly perfect agreement between experiment and calculation is obtained with the final band $f^*=f+2.5$ eV, as shown in the right panel of Fig. 6. At the Fermi level, the agreement can be made perfect if the calculated occupied *sp* band, in addition to the final-state shift, is shifted down by 0.3 eV. In Fig. 7(a) the downward shifted occupied bands are indicated by dashed lines.

This downward shift of the occupied bands is confirmed by the spectra from the upper Cu-like *d* bands taken with photon energies between 9.4 and 13 eV presented in the center panel of Fig. 5. For these photon energies the $\vec{k}$-space region around the Γ point in the second bulk BZ along [001] is sampled (see Fig. 2). Note that the direct transitions $d \rightarrow f^*$ labeled 2–4 (in Ref. 11 they were labeled 1–3) show flat-band behavior below $h\nu \approx 11.25$ (± 0.25) eV (interpolated value) and downward dispersion at higher $h\nu$. This means that the excitation at that ''critical'' photon energy occurs very close to the Γ point. Thus we denote this photon energy as $h\nu_\Gamma$, although this critical transition occurs at about 10% of $\overline{\Gamma X}$ away from Γ along Δ where the onset of the flat-band character of the initial states can be localized approximately as judged from the calculated bands. The critical Γ transition in the band structure is given in Fig. 7(a), where as initial energy that of feature 3 in Fig. 5 was taken. Within the experimental error, the agreement with final band f^* is excellent. The downward shift of the occupied band is confirmed as well.

Figure 7(a) also shows the critical transition of feature 3 near the *X* point (see also Fig. 2), which again becomes apparent by initial-state flat-band behavior now occurring at photon energy $h\nu_X \approx 20.0$ (± 0.25) eV ($E_i = -2.5$ eV). Again, the experimental final-state energy agrees with that of band f^* within the experimental error.

Finally, evidence for the final-state band f^* is also given by the inverse photoemission spectrum presented in Fig. 5(c). Peak I at final-state energy 0.5 eV above E_F, which is due to a transition into the unoccupied part of the *sp* band, cannot be understood as a transition from band *f* as the initial state, because such an interpretation would result in an absurdly large energy shift (or $\vec{k}$ shift) of the *sp* band. However, using band f^* as the initial state one gets rid of this problem. The location of the ARIPE transition is given in Fig. 6 in an expanded scale. Note that the Fermi distribution together with the broad instrumental resolution may deform peak I so that the center of the transition is by some tenth of eV at somewhat lower final energy. Even if one takes this into account (which has been done in Fig. 6 by representing peak I by the long rectangle), a shift of the *sp* band to lower energy by 0.3 eV does not appear to be justified above E_F, in contrast to the ARUPS data. However, this small inconsistency just above E_F does not influence the band mapping of the occupied states via interband transitions into f^*.

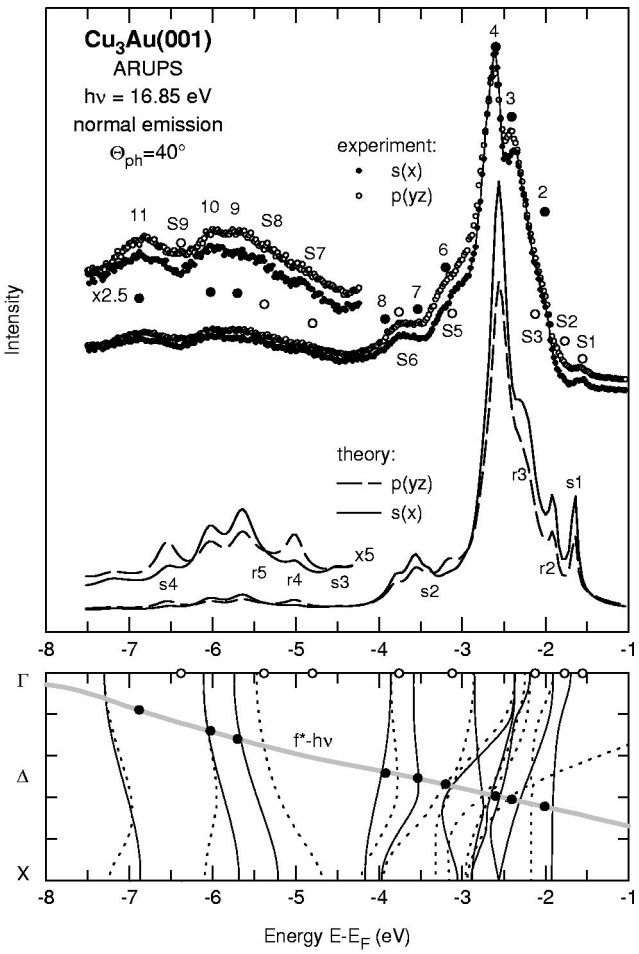

FIG. 10. Upper panel: Comparison of experimental spectra from $Cu_3Au(001)$ taken with polarized 16.9-eV radiation (data points) with the corresponding theoretical spectra obtained in the same way as those in Fig. 8. Lower panel: Calculated occupied bands of symmetry Δ_6 (dotted lines) and Δ_7 (solid lines) together with the experimental upper-state band f^* shifted downward by the photon energy. Intersections indicate theoretically possible interband transitions. The open circles (surface emissions) and the filled circles (direct transitions) represent the experimental features from the top panel.

The present energy corrections of -0.3 eV and $+2.5$ eV for the lower and the upper bands, respectively, are in line with the values -0.45 eV and $+2.05$ eV, which were determined in Ref. 7 on the grounds of spin-resolved photoemission data for only two photon energies.[34]

D. Emission from the Cu-like *d* bands

A collection of normal-emission energy-distribution curves (EDC's) from the copper *d*-like valence states between 2- and 4-eV binding energy (energy below E_F) taken in the direct transition regime with photon energies between 15.7 and 18.8 eV are shown in Fig. 8. For these photon energies, the $\vec{k}$-space region between the Γ and *X* symmetry points in the second half of the second bulk Brillouin zone

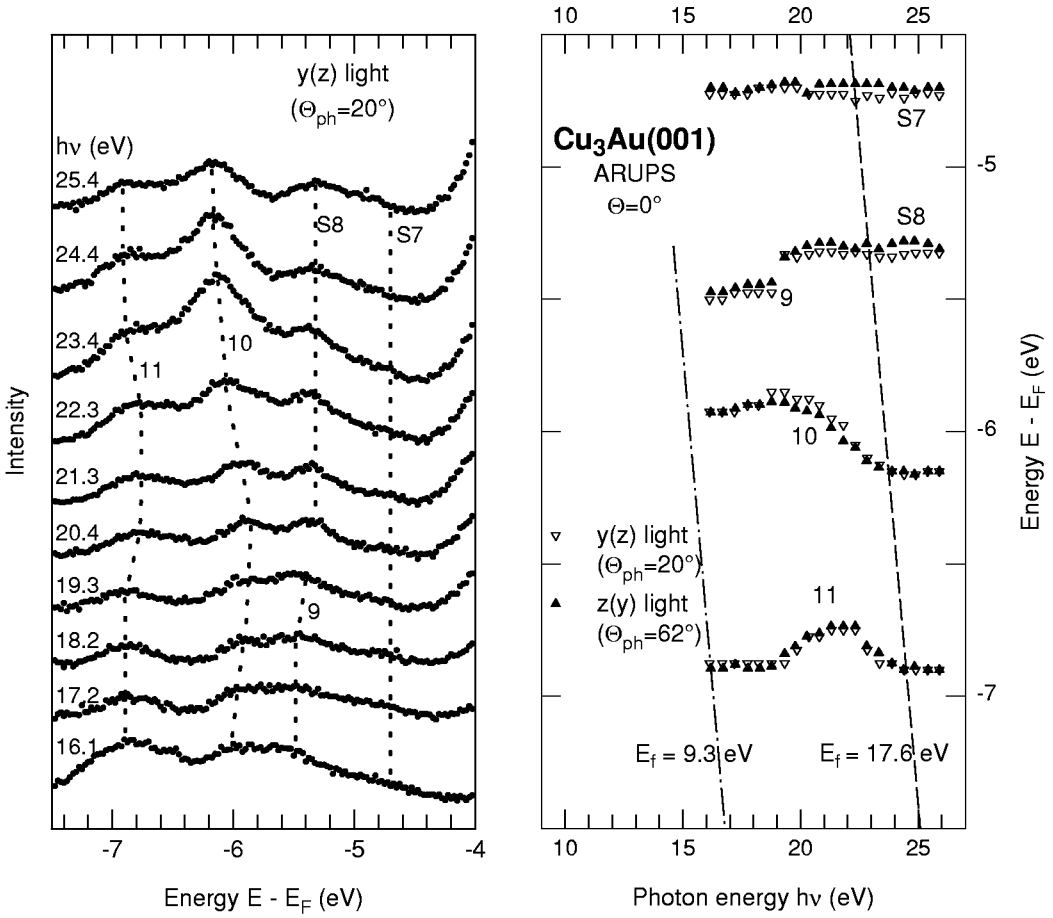

FIG. 11. Left: Series of normal-emission ARUP spectra taken from $Cu_3Au(001)$ with photon energies between 16.1 and 25.4 eV and $y(z)$ polarized synchrotron light ($\Theta_{ph}=20°$) representing the emissions from the Au-like d bands. Right: Dispersion of the Au-like emissions with photon energy.

(BBZ) along [001] (see Fig. 2) is sampled. Figure 8 also shows two theoretical spectra, which have been calculated with inner potentials comprising the final-state shift of $+2.5$ eV, which we deduced from the experimental Fermi-level crossing of the sp band, as well as the above-found initial-state shift of -0.3 eV. The agreement with the corresponding experimental spectra (16.1 and 18.3 eV, respectively) is very good for the dominating direct transition features 3 and 4. This is an impressive confirmation of our above-determined energy shifts, by which the naively calculated ''Kohn-Sham bands'' have to be corrected. Experimental and theoretical spectra agree less well in energy regions where surface emission (denoted by S) interferes with bulk emission. We attribute this to the present rather simple potential approximation in the surface region.

The dispersion of the spectral features with photon energy, including the sp-band emission, is given in Fig. 9. Some of the transitions appear as strong peaks. Others are only visible as shoulders or with weak intensity, but are clearly detected as peaks in the second derivative of the energy distribution curve (EDC) (not shown here; see Fig. 5 in Ref. 10). The pronounced intensity differences have their origin in $\vec{k}$-dependent transition matrix elements, on the one hand, and in the low-emission strength of the backfolded band of Cu_3Au as compared with Cu, on the other hand. Some features, for example, features 3 and 4 in the limited photon-energy range of Fig. 8, are immediately identified as bulk direct-transition structures by their dispersion with $h\nu$.

The character of the other features becomes evident from the energy-vs-$h\nu$ plot for the whole range investigated. This plot can roughly be divided into three regions: Left and right from the two lines of constant final energy, $E_f=9.3$ and 17.6 eV, respectively, no dispersion is observed. In between these lines, dispersion is found for the structures 1–7, which identifies them as direct transitions. At the left border of the direct transition regime the transitions into f^* occur very near the Γ point (see Figs. 4 and 7) where the initial-state bands become flat, whereas the right border corresponds to near the X point. At lower and higher photon energies the transitions approach the Γ and X point, respectively, ending in the ''tails'' of the final-state bands towards the critical symmetry points. According to the calculation shown in Figs. 4 and 6, the final-state f^* reaches the X point at about 22 eV. Dispersion of the direct transition features should thus appear well above that energy at correspondingly higher photon energies not used in our study. The energy range of the final state f^* as shown in Fig. 7 is well reproduced by the experimental data of Fig. 9. The energies of the Cu-like d bands very near the Γ and the X point can be taken immediately from that figure for photon energies below about 11 eV and above about 22 eV, respectively. Most of the additional dispersionless spectral features have been identified as

surface features (S1–S6) in a recent publication.[11] Feature 5 at $h\nu \geqslant 20$ eV is probably a density-of-states feature as has also been found in photoelectyron spectra from pure copper.[9]

Figure 10 presents a comparison between experiment and theory for spectra taken with *s*- and *p*-polarized Ne I light (16.85 eV). Over the entire range of Cu- and Au-like excitations, we observe direct transitions (marked by filled circles and numbers 2 to 11) as well as surface emissions (marked by empty circles and labels S1 to S9). We wish to stress three items. (i) The origin of the direct transitions in the band structure. For this purpose we show (in the lower panel) the calculated occupied band structure along $\Gamma\Delta X$ shifted down by 0.3 eV together with the final-states band f^* shifted down by the photon energy. Intersections between f^* and the occupied bands indicate theoretically possible direct transitions. The experimentally observed ones are represented by the filled circles. (ii) The abundance of surface emissions both in experiment (open circles) and theory. These must be identified prior to a mapping of the bulk bands, which has been done recently by us.[11] (iii) The overall good agreement between theory and experiment in the whole range of the valence bands.

E. Emission from the Au-like *d* bands

Selected spectra from the goldlike states and the dependence of the energy of the spectral features with photon energy are given in Fig. 11. As in Fig. 7 for the Cu-like states, the photon energies used scan the region between the Γ and the X points in the BBZ. Dispersion is observed for features 10 and 11, which are thus identified as direct transitions. Two features around 5-eV binding energy, S7 and S8, have been identified as surface states[11] and overlap with feature 9, which, because of its weak dispersion in its small window of observability, might also be a direct transition.

F. Experimental and calculated band structure

In Fig. 12 we present the experimental occupied band structure along $\Gamma\Delta X$, which was determined using the ''experimental'' empty band f^* and energy conservation $E_i(\mathrm{k}) = E_{f*}(\mathrm{k}) - h\nu$, where the initial energy E_i corresponds to the measured binding energy. Comparison is made with the calculated bands after rigidly shifting them downwards in energy by 0.3 eV, the value established above for the Cu-like bands.

1. Cu-like bands

Good overall agreement between experiment and theory is achieved in the region of the Cu-like bands. In particular, the dispersions of the experimental features 1 (sp band), 2–5, 7, and 8 are reproduced by theory almost exactly. The experimental structure 6 coincides with the calculated Δ_6 band from the X point to about midway of the Δ line. Going further towards the Γ point, however, it disperses much less than the calculated band. This segment (represented by empty circles in Fig. 12) is therefore likely to be not due to direct transitions from bulk states, but rather from surface states or resonances. The same holds for the data points endowed with the question mark. We also note a k dependence of differences in energy between experiment and theory. For

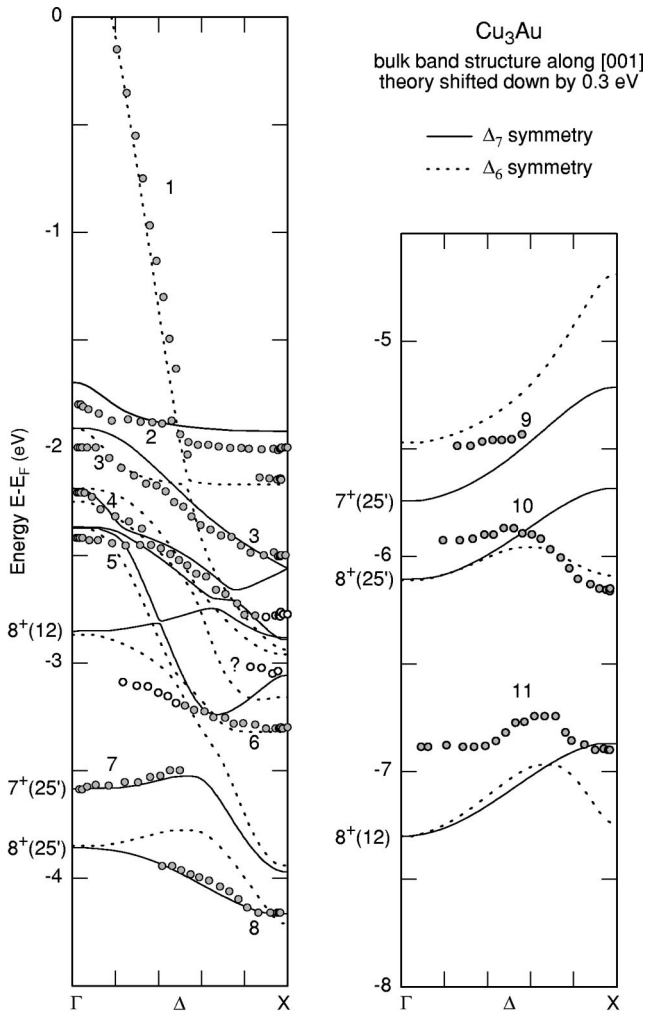

FIG. 12. Comparison between experimental and theoretical occupied band structure of Cu_3Au along [001]. The calculated bands have been shifted downward in energy by 0.3 eV. Left: Upper sp band and Cu-like d bands. Right: Au-like d bands.

example, the experimental band 2 is below the calculated one near the Γ point and beyond the midway k point, but coincides with it just left of the midway point. The rigid downward energy shift of the calculated bands by 0.3 eV is thus not equally appropriate for all bands, but has rather to be regarded as an average value. Table I summarizes the Γ point energies measured and calculated in the present work and in our previous study on $Cu_3Au(111)$.[10]

2. Au-like bands

The experimental structure 10 in Fig. 12 is seen to agree well with the calculated Δ_6 band in the right-hand part of the Δ line, but to disperse more weakly in the left-hand part. Likewise, the experimental feature 9 disperses only very weakly. Feature 11 behaves similarly. Our shift by -0.3 eV thus appears appropriate near the X point, but not in the left-hand part of the Δ line. In particular, the experimental energies near Γ are higher than the (shifted) theoretical ones (cf. also Table I) by amounts that are different for the three bands. In search for an explanation of these discrepancies, one may think of the known shortcomings of the local-

TABLE I. Γ point energies from angle-resolved photoemission experiments on $Cu_3Au(111)$ and $Cu_3Au(001)$ and from calculation with (real) Kohn-Sham potential. Energies are given in eV. (e= extrapolated; i= interference with surface emission; av = average.)

	1. Experiment		2. Theory	3. Difference of 1−2
Number (see Fig. 12)/ symmetry label	(111) (Ref. 10	(001) (this work)	(001) (this work)	
1) Cu-like *d* bands				
2		−1.81	−1.40	−0.41
3	−2.00	−2.00	−1.60	−0.40
4		−2.23	−1.88/−1.94	−0.32
5		−2.43	−2.06	−0.37
$6/8^+(12)$	−2.90	[−3.10 (i)]	−2.56	−0.34
$7/7^+(25')$	−3.62	−3.55	−3.28	−0.31
$8/8^+(25')$	−3.80		−3.55	−0.25
				−0.34 (av.)
2) Au-like bands				
9	−5.40	−5.5 (e)	−5.16	−0.34
$-/7^+(25)/t_{2g}$	−5.68		−5.43	−0.25
$10/8^+(25)/t_{2g}$	−6.00	−6.0 (e)	−5.80	−0.20
$11/8^+(12)/e_g$	−6.92	−6.90	−7.00	−0.09
				−0.22 (av.)
Average difference between experiment and theory for all bands				−0.30

density approximation for exchange and correlation in the ground state as well as of *k*-dependent real self-energy corrections.

V. SUMMARY

We have presented experimental and theoretical angle-resolved photoemission spectra (ARUPS) from the crystalline $Cu_3Au(001)$ surface. The theoretical spectra were obtained within a one-step model using a fully relativistic layer-KKR photoemission formalism. Experiment and theory agree rather well if—in addition to the imaginary potential parts describing finite electron and hole lifetimes—real inner potential corrections of −0.3 and +2.5 eV are employed in calculating the initial and final states, respectively. We recall the same findings in our photoemission study on $Cu_3Au(111)$.[10]

Using a final-state band, which was constructed from the calculated bands of dominant current with an upward shift by 2.5 eV, the direct-transition features in the experimental spectra have been evaluated to determine an experimental valence band structure along the [001] direction. In the Cu-like range, these bands and their dispersions are in good agreement with the calculated bands if the latter are shifted downward in energy by 0.3 eV. In the Au-like range, however, there are some significant discrepancies. In order to overcome these, we feel that improvements on the theoretical side are needed. In particular, one might think of going beyond the presently used local-density approximation for exchange and correlation.

ACKNOWLEDGMENTS

This work was supported by the ''Deutsche Forschungsgemeinschaft'' (SFB 166) and by the ''Bundesministerium für Bildung, Wissenschaft, Forschung und Technologie'' (BMBF Grant No. 05625PGA7). We thankfully acknowledge the skillful help of C. Zubrägel and W. Braun during the measurements at BESSY I. We also wish to thank F. Müller and R. Heise for their technical assistance.

[1] J. W. Davenport, R. E. Watson, and M. Weinert, Phys. Rev. B **37**, 9985 (1988).

[2] P. Weinberger, A. M. Boring, R. C. Albers, and W. M. Temmerman, Phys. Rev. B **38**, 5357 (1988).

[3] B. Ginatempo, G. Y. Guo, W. M. Temmermann, J. B. Staunton, and P. J. Durham, Phys. Rev. B **42**, 2761 (1990).

[4] G. S. Sohal, C. Carbone, E. Kisker, S. Krummacher, A. Fattah, W. Uelhoff, R. C. Albers, and P. Weinberger, Z. Phys. B **78**, 295 (1990).

[5] J. Kudrnovsky, S. K. Bose, and O. K. Andersen, Phys. Rev. B **43**, 4631 (1991).

[6] Z. W. Lu, S.-H Wei, and A. Zunger, Phys. Rev. B **45**, 10 314 (1992).

[7] S. V. Halilov, H. Gollisch, E. Tamura, and R. Feder, J. Phys.: Condens. Matter **5**, 4711 (1993).

[8] Z. Q. Wang, S. C. Wu, J. Quinn, C. K. C. Lok, Y. S. Li, F. Jona, and J. W. Davenport, Phys. Rev. B **38**, 7442 (1988).

[9] R. Courths and S. Hüfner, Phys. Rep. **112**, 53 (1984).

[10] M. Lau, S. Löbus, R. Courths, S. Halilov, H. Gollisch, and R. Feder, Ann. Phys. (N.Y.) **2**, 450 (1993).
[11] S. Löbus, R. Courths, S. Halilov, H. Gollisch, and R. Feder, Surf. Rev. Lett. **3**, 1749 (1996).
[12] W. Plummer and W. Eberhardt, *Advances in Chemical Physics* (Wiley, New York, 1992), Vol. 49, p. 533.
[13] F. J. Himpsel, Adv. Phys. **32**, 1 (1983).
[14] H. Wern, R. Courths, G. Leschik, and S. Hüfner, Z. Phys. B **60**, 293 (1995).
[15] R. Courths, H.-G. Zimmer, A. Goldmann, and H. Saalfeld, Phys. Rev. B **34**, 3577 (1986).
[16] S. Löbus, M. Lau, R. Courths, and S. Halilov, Surf. Sci. **287/288**, 568 (1993).
[17] U. von Barth and L. Hedin, J. Phys. C **5**, 1629 (1972).
[18] S. V. Halilov, E. Tamura, H. Gollisch, D. Meinert, and R. Feder, J. Phys.: Condens. Matter **5**, 3859 (1993).
[19] *Polarized Electrons in Surface Physics*, edited by R. Feder (World Scientific, Singapore, 1985).
[20] J. A. Knapp, F. J. Himpsel, and D. E. Eastman, Phys. Rev. B **19**, 4952 (1979).
[21] J. J. Yeh and I. Lindau, At. Data Nucl. Data Tables **32**, 1 (1985).
[22] W. Eberhardt, S. C. Wu, R. Garrett, D. Sondericker, and F. Jona, Phys. Rev. B **31**, 8285 (1985).
[23] G. K. Wertheim, Phys. Rev. B **36**, 4432 (1987).
[24] G. K. Wertheim, L. F. Mattheiss, and D. N. E. Buchanan, Phys. Rev. B **38**, 5988 (1988).
[25] S. B. DiCenzo, P. H. Citrin, E. H. Hartford, Jr., and G. K. Wertheim, Phys. Rev. B **34**, 1343 (1986).
[26] S. Krummacher, N. Sen, W. Gudat, R. Johnson, F. Grey, and J. Ghijsen, Z. Phys. B **75**, 235 (1989).
[27] P. H. Citrin, G. K. Wertheim, and Y. Baer, Phys. Rev. Lett. **41**, 1425 (1978).
[28] A. Stuck, J. Osterwalder, T. Greber, S. Hüfner, L. Schlapbach, Phys. Rev. Lett. **65**, 3029 (1990).
[29] G. Borstel, M. Neumann, and G. Wöhlicke, Phys. Rev. B **23**, 3121 (1981).
[30] *Angle-Resolved Photoemission*, edited by S. D. Kevan (Elsevier, Amsterdam, 1992), Chap. 2.
[31] S. V. Halilov, E. Tamura, H. Gollisch, R. Feder, B. Kessler, N. Müller, and U. Heinzmann, J. Phys.: Condens. Matter **5**, 3851 (1993).
[32] D. E. Eastman, J. A. Knapp, and F. J. Himpsel, Phys. Rev. Lett. **41**, 825 (1978).
[33] F. J. Himpsel and J. E. Ortega, Phys. Rev. B **46**, 9719 (1992).
[34] C. M. Schneider, G. S. Sohal, P. Schuster, and J. Kirschner, Vacuum **41**, 511 (1990).